Large-Scale Adaptive Electric Vehicle Charging

Zachary J. Lee*, Daniel Chang*, Cheng Jin†, George S. Lee†, Rand Lee*, Ted Lee†, Steven H. Low*†
*Division of Engineering & Applied Science, Caltech, Pasadena, CA
†PowerFlex Systems, Los Altos, CA.
{zlee, slow}@caltech.edu

***Abstract*—Large-scale charging infrastructure will play an important role in supporting the adoption of electric vehicles. In this paper, we address the prohibitively high capital cost of installing large numbers of charging stations within a parking facility by oversubscribing key pieces of electrical infrastructure. We describe a unique physical testbed for large-scale, high-density EV charging research which we call the Adaptive Charging Network (ACN). We describe the architecture of the ACN including its hardware and software components. We also present a practical framework for online scheduling, which is based on model predictive control and convex optimization. Based on our experience with practical EV charging systems, we introduce constraints to the EV charging problem which have not been considered in the literature, such as those imposed by unbalanced three-phase infrastructure. We use simulations based on real data collected from the ACN to illustrate the trade-offs involved in selecting models for infrastructure constraints and accounting for non-ideal charging behavior.**

I. Introduction

Electric vehicles charged with renewable energy offer the opportunity to end our reliance on polluting fossil fuels for transportation. Governments around the world have recognized this benefit and have set aggressive goals toward transitioning to electric transportation. For example, Norway has vowed to end the sale of gas and diesel cars by 2025, India by 2030, and Britain and France by 2040 [1]. In addition, California has set the goal of having 5 million electric and other zero-emission vehicles on the road by 2030 [2]. However, convenient and affordable charging infrastructure continues to be one of the greatest barriers to EV adoption [2].

While traditionally it as been assumed that EV drivers would charge overnight at their homes, a growing demographic will not have access to at home charging. In addition, to make EVs as sustainable as possible, they should be charged with renewable energy. In places like California, where solar energy is abundant, this necessitates daytime charging. For these reasons, large-scale, high-density workplace and public use charging will play an important role in the transition to EVs.

For the purpose of this paper we consider a large-scale, high-density (LSHD) charging facility to be one where 20+ EVSEs[1] share capacity constrained infrastructure. One of the primary challenges of this type of system is the cost of electrical infrastructure involved [3]. Parking facilities were not designed for the massive load imposed by EV charging and as such often require extremely expensive upgrades to transformers, utility service, etc. However, in a workplace environment, cars exhibit high flexibility, which allows us to use adaptive scheduling to defer costly infrastructure upgrades while also meeting operator objectives, such as minimizing charging delay, maximizing revenue, or following demand response signals.

In this paper we describe the development of a unique physical testbed for LSHD EV charging which we call the Adaptive Charging Network (ACN). The ACN gives us a unique platform to study practical considerations for LSHD EV charging including the behavior of users, EVs, and EVSEs. Using the ACN we can design and test algorithms using real data then explore how these algorithms perform in the wild.

Owing to to importance of EV charging research, many EV charging testbeds have been developed in the last few years. A project in the UK called My Electric Avenue was built to study the effect of at home charging on the distribution system [4]. Argonne National Lab built a testbed similar to our own but at a smaller scale (7 vs. 54 EVSEs) and used it to investigate basic adaptive control schemes [3], [5]. Likewise, UCLA developed a testbed to explore over-subscription of individual circuits using a custom 4-port charging station [6], [7]. However, none of the testbeds provide the scale and density of the ACN, which positions it as a unique resource to study LSHD deployments of charging infrastructure.

In addition, we acknowledge the wide breadth of work that has been done on algorithms for EV charging. In the interest of space, we refer the reader to surveys [8], [9] and recent work specifically related to LSHD EV charging [10]–[15]. Our work expands on this existing body of research based on our experience with real-world EV charging systems. We describe some of the more subtle constraints and considerations which must be taken into account when designing charging algorithms for LSHD EV charging systems. These include methods for dealing with unbalanced three-phase infrastructure constraints and non-ideal battery charging behavior.

The rest of this paper is organized as follows. In section II we describe the hardware and software architecture of the ACN testbed. Section III describes the our general framework for optimization based online scheduling algorithms as well as practical constraints and objective functions. We then demonstrate this online scheduling framework through simulations based on real world data from the ACN in section IV. Finally, section V concludes our work.

This material is based upon work supported by the National Science Foundation Graduate Research Fellowship under Grant No. 1745301, NSF AIR-TT under Grant No. 1602119, and NSF CTT under Grant No. 1637598.

[1]Electric vehicle supply equipment (EVSE) is the industry standard name for an electric vehicle charging station.

Fig. 1. Photograph of the ACN testbed.

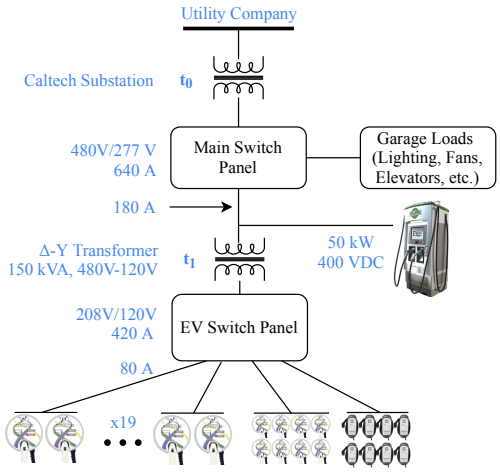

Fig. 2. System topology for the Caltech ACN testbed. This system consists of 54 6.6kW level-2 EVSEs and one 50kW DC Fast Charger. The level-2 EVSEs are fed from a 150 kVA transformer, t_1, and sub-panel. Each line connected to the EV switch panel has a capacity of 80A and is connected in a delta configuration. Nineteen of these lines feed pairs of two 32A AeroVironment EVSEs. Two additional lines feed pods of eight EVSEs each, one pod of AeroVironment stations and the other of Clipper Creek stations. The 50kW DC Fast Charger from BTC Power is a 3-phase load connected at the primary side of t_1. The EV charging circuit is connect to the main switch panel via a three-phase connection with each line capable of carrying 180 A.

II. Current ACN Testbed

In this section we describe the current state of the Caltech ACN testbed as of Spring 2018. The ACN testbed has evolved significantly since our first report in 2016 [16]. The same technology developed at Caltech has since been deployed around the country by the startup PowerFlex Systems.

A. Hardware

The Caltech ACN currently consists of 54 level-2 (208V/32A) EVSEs and one DC Fast Charger (DCFC) (400V/125A) spread across three levels of a Caltech parking garage as seen in Fig. 1. An overview of the system topology is in Fig. 2. While originally our testbed used custom EVSEs based on the OpenEVSE platform [16], we have since transitioned to commercial stations from manufactures Clipper Creek (CC) and AeroVironment (AV). These EVSEs have been modified to include a Zigbee module which can be used for two-way communication and control.

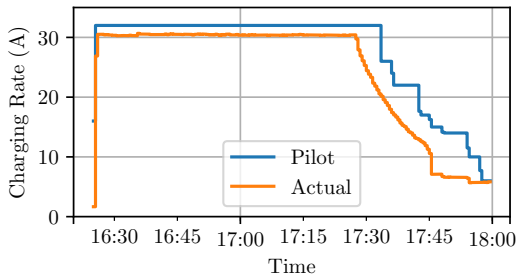

Fig. 3. Trace of the pilot signal and actual charging rate of an EV charging at the Caltech ACN. Here we see that the pilot signal always upper bounds the charging rate and that the EVs charging rate is often strictly lower than the pilot single.

We over-subscribe multiple components of our system, e.g. the 480V lines feeding transformer t_1 and the DCFC, t_1 itself, and the lines feeding each of the 8-EVSE pods. Hence, without adaptive control, it is possible that charging activities would trip the breakers protecting these components.

B. Control and Monitoring System

We have installed a dedicated industrial computer in the parking garage for monitoring and control. This computer runs custom software which acts as an intermediary between databases and algorithms running in the cloud and the physical charging hardware. Communication to individual EVSEs is accomplished with a mesh network using the Zigbee protocol, allowing for both control and data acquisition. Data is also collected from various grid health meters in the garage.

We control the charging current of each EV using the pilot signal defined in the J1772 standard [17]. This pilot signal is communicated from the EVSE to the vehicle's on-board charger and sets an upper limit on the rate at which the vehicle will charge. The vehicle can charge at any rate up to this limit. An actual charging rate below the pilot signal can occur for various reasons, e.g., the vehicle's maximum charging rate is lower than the pilot signal, the on-board charger chooses to charge more slowly to protect the battery from overheating, or the vehicle's battery is already at a high state-of-charge and requires slower charging. The actual charging rate of the vehicle is measured using a current sensor and communicated back to the controller. Figure 3 demonstrates this relationship between pilot signal and measured charging rate. Unfortunately the J1772 standard does not provide a mechanism for getting information such as state-of-charge from the vehicle, so it can be difficult to diagnose why a car is charging below its allocated pilot signal.

C. Cloud Services

Data collected from the on-site sensors, user input, and other sources are stored in time-series and relational databases in the cloud as appropriate. Scheduling algorithms and related data analysis routines are also run in the cloud. This simplifies the development and deployment of new algorithms and ensures the security of our on-site system by allowing us to maintain strict access control. Algorithms have access to all

data collected by the system through the databases mentioned above. In addition, once charging schedules have been calculated, they are placed in our time series database to be read and implemented by the on-site controller. This provides a clean interface which allows the scheduling algorithms to be decoupled from the on-site controller. All decisions made by the scheduling algorithm are stored for later analysis.

We use an event based system to trigger a call to the the scheduling algorithm. These events include a vehicle plugging in or leaving, a user changing their request parameters, or a demand response event. This is handled by a publish-subscribe model. Should none of these events occur within a set time interval (for example 10 min) we compute a new schedule anyway. These periodic computations allow the system to take into account discrepancies between the measured energy delivered and expected energy delivered which results from cars deviating from the pilot signal.

D. User Input

We use a mobile application to collect user input. This app currently allows the user to input their expected departure time and energy demand. Future iterations of the app will include the ability to enter the model of the user's car as well as willingness to pay. Taking user inputs also allows us to associate a user to each charging session. This data (in anonymized form) allows us the chance to perform learning at the level of individual users.

III. Online scheduling

In this section we describe the design of our online scheduling system. In particular, we explain the importance of some practical constraints that are often overlooked in the literature.

A. Model predictive control

The ACN computes charging rates using model predictive control, which is described in Alg. 1.

for $k \in \mathcal{K}$ **do**
(1) $\quad \mathcal{V}_k := \{i \in \hat{\mathcal{V}}_k \mid e_i(k) > 0$ **AND** $d_i(k) > 0\}$
(2) $\quad$ **if** *event fired* ***OR*** *time since last computation* $> P$ **then**
(3) $\quad\quad (r_i^*(1), ..., r_i^*(T), i \in \mathcal{V}_k) :=$ **SCH**$(\mathcal{V}_k, U_k, \mathcal{R}_k)$
(4) $\quad\quad r_i(k+t) := r_i^*(1+t),\ t = 0, \dots, T-1$
$\quad$ **end**
(5) $\quad$ set the pilot signal of EV i to $r_i(k)$, $\forall i \in \mathcal{V}_k$
(6) $\quad e_i(k+1) := e_i(k) - \hat{e}_i(k)$, $\forall i \in \mathcal{V}_k$
(7) $\quad d_i(k+1) := d_i(k) - 1$, $\forall i \in \mathcal{V}_k$
end

Algorithm 1: Model predictive control for scheduling

We use a discrete time model, with time indexed by k in $\mathcal{K} := \{1, 2, 3, ...\}$. The length of each time period is δ e.g. 1 minute. At time k, $\hat{\mathcal{V}}_k$ is the set of all EVs present at the ACN and $\mathcal{V}_k \subseteq \hat{\mathcal{V}}_k$ is the subset of *active* EVs i.e., the set of EVs whose energy demands have not been met. The state of EV $i \in \mathcal{V}_k$ at time k is described by a tuple $(e_i(k), d_i(k), \bar{r}(k))$ where $e_i(k)$ is the energy demand of the EV, $d_i(k)$ is the remaining duration of the session, and $\bar{r}(k)$ is the maximum charging rates for EV i. In addition, we define $\hat{e}(k)$ to be the measured energy delivered to the EV during time k.

We now describe the MPC algorithm. In line 1 we compute the active EV set $\mathcal{V}_k$ by looking for all EVs currently plugged in which have non-zero remaining energy demand and are not already scheduled to depart. We then check, in line 2, if we should compute a new optimal schedule. This is done whenever an event-fired flag is True, or when the time since the last computed schedule exceeds P time periods.

If a new schedule is required, we call the optimal scheduling algorithm **SCH** in line 3 that is defined by three parameters $(\mathcal{V}_k, U_k, \mathcal{R}_k)$ and takes the form:

$$\max_{\hat{r}} \quad U_k(\hat{r}) \tag{1a}$$
$$\text{s.t.} \quad \hat{r} \in \mathcal{R}_k \tag{1b}$$

The set $\mathcal{V}_k$ of active EVs defines the optimization variable $\hat{r} := (\hat{r}_i(1), \dots, \hat{r}_i(T), i \in \mathcal{V}_k)$ for every active EV i over the optimization horizon $\mathcal{T} := \{1, \dots, T\}$. The utility function U_k encodes various objectives and the feasible set R_k encodes various constraints. They will be discussed in detail in the next two subsection. Note that **SCH** does not have a notion of the current time k and returns an optimal solution $r_i^* := (r^*(1), ..., r^*(T))$ of (1) as a T-dimensional vector. The algorithm then adjusts the indexing and set the scheduled charging rates of EVs i at time k as $r_i(k+t) := r_i^*(1+t)$, $t = 0, ..., T-1$ in line 4. At every time k, regardless of if a new schedule was produced, we set the pilot signal of each EV i to $r_i(k)$ (line 5) and update the state parameters (lines 6, 7) for the next time period.

We now describe in detail how to design the utility function U_k to achieve desirable features and how to model various constraints that define the feasible set $\mathcal{R}_k$ for practical systems.

B. Utility Functions U_k

We allow the utility function to change for each computation, but to simplify notation we drop the subscript k. The utility functions we adopt are a weighted sum of two components:

$$U(r) \quad := \quad V_{op}(r) - \alpha V_{reg}(r)$$

where $V_{op}(r)$ captures operator objectives, $V_{reg}(r)$ is a regularizer to promote secondary desirable properties, and $\alpha \geq 0$ is a weight.

1) Operator objectives V_{op}: The utility function $V_{op}(r)$ can encode many operator objectives. For example, let $p(t)$ and $c(t)$ be the time-varying revenue and cost of one unit of energy respectively and Δ be a demand charge which is charged by the utility based on the maximum power draw in a billing period. The problem of maximizing profit can then be formulated with the following utility function:

$$V_{op}(r) \quad := \quad \sum_{\substack{t \in \mathcal{T} \\ i \in \mathcal{V}}} (p(t) - c(t)) r_i(t) \ - \ \Delta \cdot \max\left(\max_{t \in \mathcal{T}} \left(\sum_{i \in \mathcal{V}} r_i(t) + L^{aux}(t) \right), L_0^{max} \right)$$

where $\mathcal{V}$ is the set of active EVs and $\mathcal{T} := \{1, \dots, T\}$ is the optimization horizon. Here $L^{aux}(t)$ denotes the draw of the other loads which share a meter with the ACN. To account for usage outside our control horizon, we denote by L_0^{max} the highest peak for this billing period so far.

Another example is to encourage EVs to charge as quickly as possible using the utility function:

$$V_{op}(r) := \sum_{t \in \mathcal{T}} (T - t) \sum_{i \in \mathcal{V}} r_i(t) \tag{2}$$

This serves to minimize charging delay as well as free up capacity for future arrivals.

Yet another example is to track a given load profile $D(t)$ using the utility function:

$$V_{op}(r) := -\sum_{t \in \mathcal{T}} \left(\sum_{i \in \mathcal{V}} r_i(t) + L^{aux}(t) - D(t) \right)^2$$

This may be necessary when trying to maximize the utilization of on-site renewable energy resources or when the site operator has entered into an agreement with the utility to maintain a scheduled load profile.

2) Regularizers V_{reg}: In addition to operator objectives, we also include regularizers to promote other desirable properties. For example, we can smooth the charging rates across time by including the regularizer:

$$V_{reg}(r) := \sum_{i \in \mathcal{V}} \left(\sum_{t \in \mathcal{T}} (r_i(t) - r_i(t-1))^2 \right)$$

where we define $r_i(0)$ to be the charging rate in the time period immediately before the current computation. For EVs who have not been charging previously we omit the regularizer for the first rate. A smoothed charging schedule is desirable as it discourages rapid fluctuations between zero and non-zero rates which can cause contactor wear and lead to EV error states as well as confuse users.

The utility functions described so far are not strictly concave in r and hence there is generally nonunique optimal solution r^*. We can force a unique optimal solution by including the regularizer:

$$V_{reg}(r) := \sum_{\substack{t \in \mathcal{T} \\ i \in \mathcal{V}}} r_i^2(t)$$

This regularizer also promotes equal sharing among the EVs.

C. Feasible set $\mathcal{R}_k$

The feasible set $\mathcal{R}_k$ is defined by a set of equality and inequality constraints that can depend on k, but for notational simplicity, we drop the subscript k. These constraints then take the form:

$$0 \leq r_i(t) \leq \bar{r}_i(t) \qquad t < d_i, i \in \mathcal{V} \tag{3a}$$

$$r_i(t) = 0 \qquad t \geq d_i, i \in \mathcal{V} \tag{3b}$$

$$\sum_{t=a_i}^{d_i - 1} r_i(t)\delta \leq e_i \qquad i \in \mathcal{V} \tag{3c}$$

$$f_j(r_1(t), ..., r_N(t)) \leq R_j(t) \qquad t \in \mathcal{T}, j \in \hat{\mathcal{R}} \tag{3d}$$

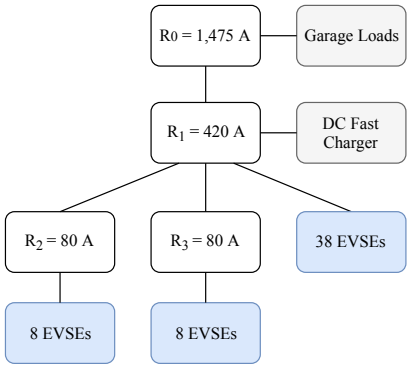

Fig. 4. Simple abstraction of constraints for the Caltech ANC Testbed. Here we treat the testbed as if it were a single phase system. All constraints have been translated to the secondary side of transformer t_1. The top level constraint (R_0) encodes the rating of t_0, the main transformer supplying the parking garage. Constraint R_1 comes from the line feeding transformer t_1 and the DCFC from the main panel. This constraint has been sized such that it also enforces the capacity of t_1. Constraints R_2 and R_3 each represents the constraints on the lines feeding each of the 8-EVSE pods. We do not need to model the line constraint for the EVSE pairs, as the maximum current draw of both stations (64 A) is less than the line limit (80 A).

Constraints (3a) ensure that the charging rate in each period is nonnegative and below the maximum charging rate $\bar{r}_i(t)$ of the EV. Constraints (3b) ensure that an EV does not charge after its departure time. We use constraints (3c) to limit the total energy delivered to EV i to at most e_i, because of this inequality, care should be taken when designing the utility function so that its optimal solution does not result in a zero rate vector (i.e. minimizing cost).[2] Finally constraint (3d) enforces a set of infrastructure limits indexed by $j \in \hat{\mathcal{R}}$. For each constraint j, $R_j(t)$ is a given capacity limit for time t, $f_j : \mathbb{R}_+^N \to \mathbb{R}_+$ is a convex function that maps a rate vector $r(t)$ for all active EVs to an aggregate rate $f_j(r(t))$, and we require that the aggregate rate $f_j(r(t))$ does not exceed the capacity $R_j(t)$. This models the situation where a set of EVs share a resource j with capacity $R_j(t)$ at time t. The function f_j depends on the layout of ACN. We next describe these infrastructure constraints in detail.

1) Single-phase infrastructure constraints: As mentioned in Section II-A, several components in our testbed have been over-subscribed. These over-subscriptions can be encoded as constraints for our scheduling problem. An abstraction of these constraints is shown in Fig. 4 and explained in the caption of the figure. We express all constraints as current constraints reflected to the secondary side of t_1. This allows us to easily relate the constraints to our control variables, which are the charging rates, in amps, of the EVSEs. We treat the garage loads and the DCFC as uncontrollable loads, the power draw of which is subtracted from R_0 and R_1 respectively.

This abstraction is commonly modeled as a set of linear constraints in the literature, as follows. Let S_j be the set of all EVSEs which are subject to capacity limit $R_j(t)$ (below

[2]For more general utility functions, this constraint can be tightened to an equality, though care must be taken to deal with possible infeasibility. We do not discuss this here in the interest of space.

node R_j in Fig. 4). Then the constraints on the charging rates are usually expressed as

$$\sum_{i \in S_j} r_i(t) \leq R_j \quad \forall j \tag{4}$$

While this model is widely used, it is suitable only when all EVSEs are on a single phase.

In practice, however, EVSEs are usually connected on three-phase circuits. In this case, the constraints (4) are too conservative and will underutilize the resource by up to 42.3%.

2) Unbalanced three-phase infrastructure constraints: The EVSEs in Caltech ACN are connected in a delta configuration as shown in Fig. 5. Because of differences in demand the loads in this delta configuration are often imbalanced which requires us to carefully consider the infrastructure constraints to ensure safe operation. For modeling simplicity, we assume that the line impedances leading to each station are negligible, allowing us to lump all EVSEs between common phases into a single load represented by current phasors $I_{ab}^{evse}, I_{bc}^{evse}, I_{ca}^{evse}$. We also assume that each EVSE is modeled as a controllable current source with unity power factor. With this model we must consider two types of constraints:

- *Phase Constraints*: A phase constraint pertains to the current along one leg of the delta, i.e. ab, bc, or ca. For example constraints on the aggregate current of the AV and CC pods are phase constraints in the Caltech ACN. Since we can treat the EVSEs within the same phase as in parallel and all have unity power factor, we can express the constraint as (4).
- *Line Constraints*: A line constraint pertains to the current along each line i.e. a, b, or c. Examples of line constraints in the Caltech ACN include limits on I_p^0, I_p^1, I_p^2 and I_p^3 where $p \in \{a, b, c\}$.

We now explain how to derive the constraints on these current magnitudes $|I_p^0|, |I_p^1|, |I_p^2|$, and $|I_p^3|, p \in \{a, b, c\}$, using the circuit diagram in Fig. 5. We can calculate the line currents I_p^3 from the phase currents:

$$\begin{aligned} I_a^3 &= I_{ab}^{evse} - I_{ca}^{evse} \\ I_b^3 &= I_{bc}^{evse} - I_{ab}^{evse} \\ I_c^3 &= I_{ca}^{evse} - I_{bc}^{evse} \end{aligned} \tag{5}$$

where each variable is a phasor. From this point on we will only consider one phase/line in the interest of space, but all other constraints follow from this derivation. To find I_{ab}^{evse} we define the set of all EVSEs connected between lines a and b to be S_{ab}, likewise for bc and ca. We can then define the magnitude of the aggregate phase current for *each* leg of the delta as

$$|I_{ab}^{evse}| := \sum_{i \in S_{ab}} r_i(t) \tag{6}$$

We treat each EVSE as a constant current load with unity power factor, so the phase of each current matches the phase of the corresponding voltage. We assume that we are able to measure/calculate the phase angle of the voltage across each leg of the delta configuration. We denote the phase angle of each phase as ϕ_{ab}, ϕ_{bc}, and ϕ_{ca} respectively. If measurements of voltage phase angles are not available, we assume that voltage angles are balanced, i.e., each phasor is spaced 120° apart. In any case, we emphasize that in the phasor

$$I_{ab}^{evse} = |I_{ab}^{evse}| \cdot e^{j\phi_{ab}} \tag{7}$$

only the magnitude $|I_{ab}^{evse}|$ is variable and the phase $e^{j\phi_{ab}}$ is known.

From (5), the current constraint $|I_a^3| \leq R_{3,a}$ becomes a constraints on I_{ab}^{evse} and I_{ca}^{evse}:

$$|I_a^3| \;=\; |\, I_{ab}^{evse} - I_{ca}^{evse}\,| \;\leq\; R_{3,a} \tag{8a}$$

Note that this constraint is a second-order cone (SOC) constraint in the magnitudes $|I_{ab}^{evse}|, |I_{ca}^{evse}|$. To see this, notice

$$\begin{aligned} |I_{ab}^{evse} - I_{ca}^{evse}|^2 \;=\; & (|I_{ab}^{evse}| \cos\phi_{ab} - |I_{ca}^{evse}| \cos\phi_{ca})^2 \;+ \\ & (|I_{ab}^{evse}| \sin\phi_{ab} - |I_{ca}^{evse}| \sin\phi_{ca})^2 \end{aligned}$$

In order to account for constraints on I_a^2, I_a^1 and I_a^0 we must consider the effect of the delta-wye transformer t_1. Using circuit analysis we can relate I_a^2 to the aggregated EVSE currents:

$$I_a^2 \;=\; \frac{1}{n}(I_{ab}^{evse} + I_{bc}^{evse} - 2I_{ca}^{evse})$$

where n is the turns ratio of the transformer which in our system is 4. Hence the constraint on I_a^2 can be expressed in terms of EVSE current magnitudes as:

$$|I_a^2| \;=\; \frac{1}{n}\,|I_{ab}^{evse} + I_{bc}^{evse} - 2I_{ca}^{evse}| \;\leq\; R_{2,a} \tag{8b}$$

where $R_{2,a}$ is expressed as a current constraint on the primary side of t_1, rather than reflecting it to the secondary side as was done in Section III-C1.

Finally, we can obtain I_a^1 and I_a^0 from I_a^2 by adding the currents drawn from the DC fast charging and the auxiliary garage loads. Hence its constraints are:

$$\left|\frac{1}{n}(I_{ab}^{evse} + I_{bc}^{evse} - 2I_{ca}^{evse}) + I_a^{DC}\right| \;\leq\; R_{1,a} \tag{8c}$$

$$\left|\frac{1}{n}(I_{ab}^{evse} + I_{bc}^{evse} - 2I_{ca}^{evse}) + I_a^{DC} + I_a^{aux}\right| \;\leq\; R_{0,a} \tag{8d}$$

Like (8a), the constraints (8b), (8c) and (8d) are SOC constraints. These constraints translate into constraints on the charging rates $r_i(t)$ through (6).

In some applications these SOC constraints are too computationally expensive, however. Simpler but more conservative constraints can be derived by observing

$$|I_a^3| \;=\; |I_{ab}^{evse} - I_{ca}^{evse}| \;\leq\; |I_{ab}^{evse}| + |I_{ca}^{evse}|$$

Hence the constraints (8) can be relaxed to:

$$|I_{ab}^{evse}| + |I_{ca}^{evse}| \;\leq R_{3,a} \tag{9a}$$

$$\frac{1}{n}(|I_{ab}^{evse}| + |I_{bc}^{evse}| + 2|I_{ca}^{evse}|) \;\leq R_{2,a} \tag{9b}$$

$$\frac{1}{n}(|I_{ab}^{evse}| + |I_{bc}^{evse}| + 2|I_{ca}^{evse}|) + I_a^{DC} \;\leq R_{1,a} \tag{9c}$$

$$\frac{1}{n}(|I_{ab}^{evse}| + |I_{bc}^{evse}| + 2|I_{ca}^{evse}|) + I_a^{DC} + I_a^{aux} \;\leq R_{0,a} \tag{9d}$$

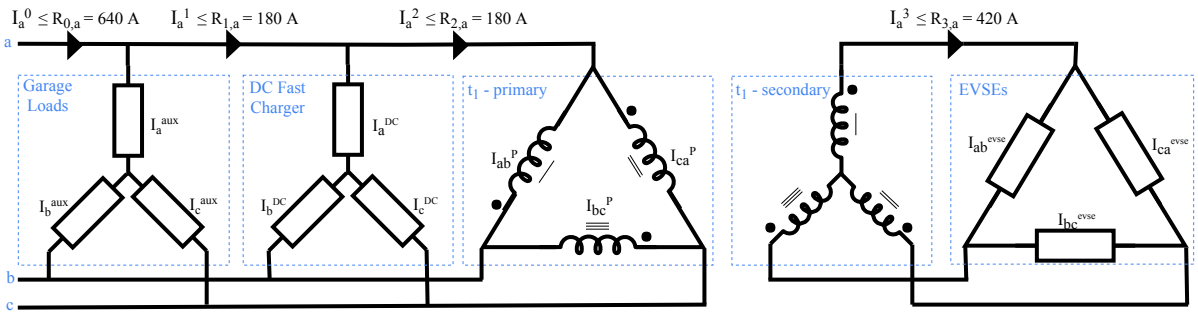

Fig. 5. Circuit diagram of Caltech ACN.

TABLE I
SUMMARY STATISTICS FOR EV CHARGING TEST CASES
APRIL 15-21, 2018

	Total Sessions	Mean Duration (hours)	Mean Energy (kWh)	Total Energy (kWh)	Max Concurrent Sessions
Sun	26	2.71	9.74	253.34	8
Mon	52	6.31	9.66	502.57	33
Tues	56	5.91	8.61	481.99	35
Wed	63	5.70	8.15	513.55	37
Thurs	45	6.65	8.96	403.27	32
Fri	53	6.12	9.71	514.64	33
Sat	27	3.93	9.96	269.04	11
Total	322	5.33	9.26	2,938.39	37

IV. SIMULATIONS

In this section we demonstrate the usefulness of the online scheduling framework described in section III using simulations based on real data collected from the ACN. We use simulations rather than real world traces from our system as it is easier to demonstrate the effects of different parameters in a controlled simulation environment. For simplicity in these simulations we do not include auxiliary loads such the DCFC or garage loads.

A. Test Cases

For these simulations we use data collected from the ACN for the week of April 15 - April 21, 2018 totaling 322 individual charging sessions and 2.94 MWh of energy delivered. For each session the dataset we have plug-in time, unplug time, total energy delivered, and station id. Table IV-A shows summary statistics for this dataset.

B. Effect of Infrastructure Constraints

In our first experiment, we demonstrate that the second order cone formulation of infrastructure constraints is beneficial in highly constrained systems, while the affine bound is sufficient in less constrained settings.

The setup of this experiment is as follows. We set $P = \delta = 5$ minutes and use utility function (2) which promotes charging as quickly as possible. We denote the charging schedule when using the SOC constraints in (8) as r_{soc} and the schedule with affine constraints in (9) as r_{aff}.

To demonstrate the effect of constrained infrastructure, we artificially limit the capacity of the infrastructure limits $R_{2,p}$ and $R_{3,p}$, $p \in \{a, b, c\}$ to a percentage of their nominal value. We do not consider $R_{0,p}$ or $R_{1,p}$ as we have ignored the DCFC and garage loads.

We show the results of this simulation in Fig. 6. Fig. 6(a) shows the results on a single day, April 18. As expected, as infrastructure constraints become tighter, the objective function decreases for both cases, however the SOC constraints are able to maintain a significantly higher objective value even in highly constrained settings. This trend holds for all days in our test set, as seen in Fig. 6(b).

The choice between these constraint formulations is thus a function of both the state and size of the system as well as performance constraints on the algorithm. For systems where infrastructure is not highly oversubscribed, affine constraints are likely good enough. For highly constrained systems, SOC constraints offer some benefits but at the cost of longer compute time. In our experiments using Gurobi 8.0.0 [18] we found that the the mean (max) solve time of each instance of **SCH** with SOC constraints takes only 28 ms (264 ms) vs 6.7 ms (64.4 ms) with affine constraints on a machine with a 2.8 GHz 7^{th} generation Intel i7 processor and 16 GB RAM. Thus this trade-off may only be important for large problem instances (large numbers of EVSEs and small δ values) or when running many successive simulations.

C. Effect of Non-Ideal Charging Behavior

We next demonstrate how periodic recomputation can be used to help account for non-ideal charging behaviors. For this simulation we once again use δ = 5 minutes and the utility function (2). We use SOC infrastructure constraints.

We consider a two-stage battery charging model. The first stage, referred to as *bulk* charging, occurs up to 80% state of charge. In this stage current draw, neglecting changes in pilot, is near constant. The second stage, called *absorption*, finishes charging the remaining 20%. In this stage, current decreases as the battery reaches full charge. For simplicity we consider a piecewise linear model where current during the bulk charging period is limited to 32 A, and current in the absorption charging period decreases linearly from 32 A to 0 A. Since both the initial state of charge and the battery capacity are unknown, we assume that we are in the bulk charging stage

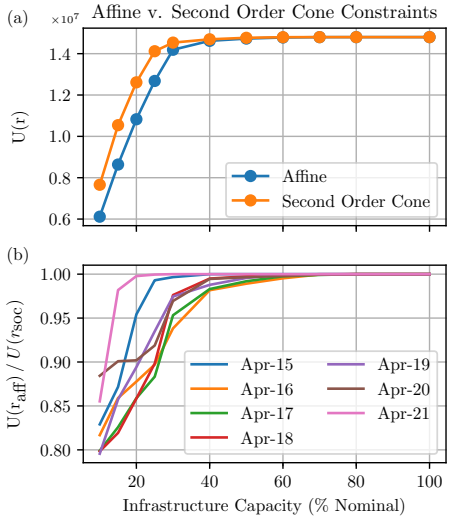

Fig. 6. Comparison of the utility obtained by schedules found using second order cone and affine infrastructure constraints. (a) Maximum utility obtained by using **SCH** with SOC or affine constraints for varying infrastructure capacities on Apr. 18, 2018. (b) Ratio of utility for the optimal schedule produced with affine constraints over the utility with SOC constraints for the week of April 15-21, 2018. In both cases we see that affine constraints are adequate for lightly constrained systems, while SOC constraints increase utility in highly constrained settings.

for the first 80% of energy delivered in the session and in the absorption stage for the remaining 20%.

We model additional deviation from this simplified model as additive zero mean Gaussian noise. With this model, the actual charging rate of an EV i with pilot $r_i(k)$ is given by

$$\hat{r}_i(t) := \begin{cases} r_i(t) - |x| & \text{if } \frac{e_i(k)}{e_i(0)} \leq 0.8 \\ \min\left(\left(1 - \frac{e_i(k)}{e_i(0)}\right)\frac{32}{0.2} + x,\ r_i(t)\right) & \text{otherwise} \end{cases}$$

where $x \sim \mathcal{N}(0, \sigma^2)$.

Once again we consider a single day, April 18. The results of this experiment are shown in Fig. 7. We observe that in the ideal case the maximum recompute period has no effect, meaning we can recompute only when an event occurs. However, as the two-stage charging model is introduced and noise increases, having lower P values becomes more important. Thus, in real systems, designers should push P as low as possible while still ensuring that they can finish all necessary computation and communication within the period.

V. Conclusions

In this work we have introduced the Adaptive Charging network, a unique physical testbed which allows us evaluate EV charging algorithms and collect valuable real-world charging data. We explain the architecture of this system including hardware and software components. We also introduce a general framework for online EV charging algorithms including a novel formulation of unbalanced 3-phase infrastructure constraints. Finally we use real data from the ACN in simulations to demonstrate the effects of different components of the algorithm framework. In the future, we plan to use the ACN

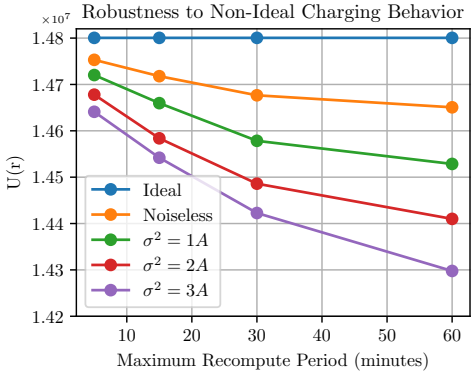

Fig. 7. Effect of non-ideal charging behavior on the scheduling problem. We consider five charge behaviors including an ideal charging model with no absorption stage or noise and four versions of the two-stage model different levels of Gaussian noise. We see that using smaller maximum recompute periods can help to mitigate the effect of non-ideal charging behavior.

to continue collecting data, build models of user behavior, and demonstrate participation in demand response programs.

References

[1] A. Petroff, "These countries want to ditch gas and diesel cars," June 2017.

[2] S. of California, "Climate Change Investment Plan," 2018.

[3] T. Bohn, C. Cortes, and H. Glenn, "Local automatic load control for electric vehicle smart charging systems extensible via OCPP using compact submeters," pp. 724–731, IEEE, June 2017.

[4] J. Cross and R. Hartshorn, "My Electric Avenue: Integrating Electric Vehicles into the Electrical Networks," pp. 12 (6 .)–12 (6 .), Institution of Engineering and Technology, 2016.

[5] T. Bohn and H. Glenn, "A real world technology testbed for electric vehicle smart charging systems and PEV-EVSE interoperability evaluation," pp. 1–8, IEEE, Sept. 2016.

[6] J. Chynoweth, Ching-Yen Chung, C. Qiu, P. Chu, and R. Gadh, "Smart electric vehicle charging infrastructure overview," pp. 1–5, IEEE, Feb. 2014.

[7] C.-Y. Chung, J. Chynoweth, C.-C. Chu, and R. Gadh, "Master-Slave Control Scheme in Electric Vehicle Smart Charging Infrastructure," *The Scientific World Journal*, vol. 2014, pp. 1–14, 2014.

[8] Q. Wang, X. Liu, J. Du, and F. Kong, "Smart Charging for Electric Vehicles: A Survey From the Algorithmic Perspective," *IEEE Communications Surveys & Tutorials*, vol. 18, no. 2, pp. 1500–1517, 2016.

[9] J. C. Mukherjee and A. Gupta, "A Review of Charge Scheduling of Electric Vehicles in Smart Grid," *IEEE Systems Journal*, vol. 9, pp. 1541–1553, Dec. 2015.

[10] S. Chen and L. Tong, "iEMS for large scale charging of electric vehicles: Architecture and optimal online scheduling," pp. 629–634, IEEE, Nov. 2012.

[11] Z. Yu, S. Chen, and L. Tong, "An intelligent energy management system for large-scale charging of electric vehicles," *CSEE Journal of Power and Energy Systems*, vol. 2, pp. 47–53, Mar. 2016.

[12] Z. Yu and L. Tong, "Demand response via large scale charging of electric vehicles," pp. 1–5, IEEE, July 2016.

[13] L. Guo, K. F. Erliksson, and S. H. Low, "Optimal online adaptive electric vehicle charging," pp. 1–5, IEEE, July 2017.

[14] Y. Nakahira, N. Chen, L. Chen, and S. H. Low, "Smoothed Least-laxity-first Algorithm for EV Charging," pp. 242–251, ACM Press, 2017.

[15] B. Wang, Y. Wang, H. Nazaripouya, C. Qiu, C.-c. Chu, and R. Gadh, "Predictive Scheduling Framework for Electric Vehicles Considering Uncertainties of User Behaviors," *IEEE Internet of Things Journal*, pp. 1–1, 2016.

[16] G. Lee, T. Lee, Z. Low, S. H. Low, and C. Ortega, "Adaptive Charging Network for Electric Vehicles," in *2016 IEEE Global Conference on Signal and Information Processing*, Dec. 2016.

[17] SAE, "SAE Electric Vehicle and Plug in Hybrid Electric Vehicle Conductive Charge Coupler J1772_201710," 2017.

[18] I. Gurobi Optimization, *Gurobi Optimizer Reference Manual*. 2016.